Journal of Dental Research
1–9

DOI: 10.1177/0022034514566029
jdr.sagepub.com

Multiscale Analyses of the Bone-implant Interface

J.Y. Cha[1,2], M.D. Pereira[1], A.A. Smith[1], K.S. Houschyar[1], X. Yin[1,3], S. Mouraret[1], J.B. Brunski[1], and J.A. Helms[1]

Abstract

Implants placed with high insertion torque (IT) typically exhibit primary stability, which enables early loading. Whether high IT has a negative impact on peri-implant bone health, however, remains to be determined. The purpose of this study was to ascertain how peri-implant bone responds to strains and stresses created when implants are placed with low and high IT. Titanium micro-implants were inserted into murine femurs with low and high IT using torque values that were scaled to approximate those used to place clinically sized implants. Torque created in peri-implant tissues a distribution and magnitude of strains, which were calculated through finite element modeling. Stiffness tests quantified primary and secondary implant stability. At multiple time points, molecular, cellular, and histomorphometric analyses were performed to quantitatively determine the effect of high and low strains on apoptosis, mineralization, resorption, and collagen matrix deposition in peri-implant bone. Preparation of an osteotomy results in a narrow zone of dead and dying osteocytes in peri-implant bone that is not significantly enlarged in response to implants placed with low IT. Placing implants with high IT more than doubles this zone of dead and dying osteocytes. As a result, peri-implant bone develops micro-fractures, bone resorption is increased, and bone formation is decreased. Using high IT to place an implant creates high interfacial stress and strain that are associated with damage to peri-implant bone and therefore should be avoided to best preserve the viability of this tissue.

Keywords: dental implantation, prosthesis implantation, orthodontic anchorage techniques, finite element analysis, osseointegration, biological process

Introduction

Implants—whether used in orthodontic practice as anchorage devices or in prosthodontics to replace missing teeth—require osseointegration to be functional (Higuchi and Block 2000). For example, orthodontic mini-implants must be osseointegrated to serve as anchors in the attempt to intrude or retract maxillary incisors or move teeth in a mesial direction (Deguchi et al. 2003). Likewise, dental implants must be osseointegrated to withstand masticatory forces (Esposito et al. 2013).

Implant stability is frequently used as a measure of successful osseointegration, but quantifying stability at the time of implant placement is difficult. One method to infer stability is to directly measure the insertional torque (IT) required to place the implant. IT values, measured in Newton centimeters (N-cm), are influenced by bone quality and quantity at the insertion site (Cha et al. 2010) and by the diameter of the implant relative to the diameter of the osteotomy (Norton 2013). Higher IT may contribute to primary stability of the implant, but there is also an associated risk of damaging the interfacial bone due to increased strain (Trisi et al. 2011). Some investigators assert that when IT values are high, necrosis and micro-fracture of interfacial bone occur (Duyck et al. 2010).

Here, using a small animal model coupled with finite element (FE) analyses, we predicted the distribution and magnitude of interfacial stresses and strains generated by high and low IT and correlated these with the subcellular, cellular, and tissue responses. Our multiscale analyses revealed a strong correlation between high IT and large interfacial compressive

[1]Division of Plastic and Reconstructive Surgery, Department of Surgery, Stanford School of Medicine, Stanford, CA, USA
[2]Orthodontic Department, College of Dentistry, Yonsei University, Seoul, South Korea
[3]State Key Laboratory of Oral Disease, West China Hospital of Stomatology, Sichuan University, Chengdu, China

A supplemental appendix to this article is published electronically only at http://jdr.sagepub.com/supplemental.

Corresponding Author:
J.A. Helms, Stanford University, 257 Campus Dr., Stanford, CA 94305, USA.
Email: jhelms@stanford.edu

strains, broader zones of programmed cell death, extensive osteoclast remodeling, and microdamage in the bone. In contrast, implants placed with low IT showed significantly smaller compressive strains, minimal cell death, robust osteogenesis, and an increase in primary stability over time. These findings have direct implications for successful osseointegration of implants in humans.

Materials and Methods

Description of Implant

All procedures were approved by the Stanford Administrative Panel on Laboratory Animal Care and conform to the ARRIVE (Animal Research: Reporting of In Vivo Experiments) guidelines. Adult wild-type male mice were anaesthetized; an incision extending from the lateral knee to proximal hip was made; a flap was elevated; and a low-speed dental engine was used to create a pilot osteotomy with 0.30- to 0.57-mm drill bits (Drill Bit City, Chicago, IL). The site was rinsed, and a titanium-6 aluminum-4 vanadium alloy implant (NTI Kahla GmbH, Germany) was inserted. The flap was closed. Animals were divided into treatment groups as shown in the Appendix Figure.

Measurement of IT

A torque gauge (Tohnichi, Japan) was calibrated to known values; metal shims were suspended at a fixed distance off an allen wrench clamped in the 3-jaw chuck of the torque gauge. By varying the weight of the metal shims, a series of known torques were delivered to the torque gauge. After validation, the torque gauge was used to measure IT; the procedure was repeated twice.

Tissue Preparation and Immunostaining

Tissues were prepared as described (Leucht et al. 2007). Histologic stains, alkaline phosphatase (ALP), tartrate-resistant acid phosphatase (TRAP) activity, and Picrosirius red staining were performed as described (Leucht et al. 2007). TUNEL (Roche, Indianapolis, IN) was performed as described by the manufacturer. Immunohistochemistry for Runx2 and PCNA was carried out as described (Minear et al. 2010).

Histomorphometric Analyses

Thirty-two implants were analyzed; 16 were placed with high IT and 16 with low IT. From the 32 IT samples, half were stained for TUNEL. Each sample was sectioned through in its entirety and all slides stained for TUNEL. Each slide was photographed at 40× and archived. On each image, the distance from the edge of the osteotomy to the $TUNEL^{+ve}$ and $DAPI^{+ve}$ cells was measured. Multiple measurements were made in each quadrant around the implant. Measurements were averaged. For histomorphometric measurements of Runx2 and PCNA, the peri-implant space was evaluated at 20× and divided into 4 microscopic fields of view. Within each microscopic field of view, $Runx2^{+ve}$ cells were selected with the magic wand function of Adobe Photoshop. This allowed for the conversion of positive cells into positive pixels that corresponded to the Runx2-expressing cells. The same procedure was followed for PCNA.

Bone-implant Stiffness Analyses

The bone-implant stiffness test was based on general mechanics theory where the deflection of an end-supported cantilever beam is given by the following equation:

$$\delta = \frac{FL^3}{3EI},$$

where F is load, L is beam length, E is Young modulus, I is moment of inertia of the beam, and δ is the beam's deflection at its tip. To measure defection, femurs containing implants were clamped in an alligator clip rigidly attached to a solid support and positioned between a stepper motor and a transducer for measuring displacements. Stiffness was computed by modeling the implant as a cantilever beam, as above, and computing the quantity EI (see Results). Two groups of implants were analyzed: those that had been in place for 1 d (n = 5 for high IT and 5 for low IT) and implants that had been in place for 7 d (n = 5 high IT and 5 low IT).

Statistical Analyses

IT is presented in the form of mean ± standard deviation. A nonparametric Wilcoxon test was used to analyze all histomorphometric analyses. A 2-way analysis of variance was used in the stiffness testing. Significance was attained at $P < 0.05$, and all statistical analyses were performed with SPSS 20.

Results

Preparing an Osteotomy Creates a Narrow Zone of Dead and Dying Osteocytes

Before assessing how IT affected peri-implant bone health, we first had to evaluate how the osteotomy affected bone viability. We prepared osteotomies (arrows, Fig. 1A) and then 24 h later used DAPI staining to identify live osteocytes (Fig. 1B). Dead osteocytes were identified by the lack of DAPI staining in the lacunae (red arrowheads, Fig. 1B). Dying osteocytes were $TUNEL^{+ve}$ (white arrows, Fig. 1B). A ~70-μm-wide zone of dead and dying osteocytes was identified around the osteotomy site.

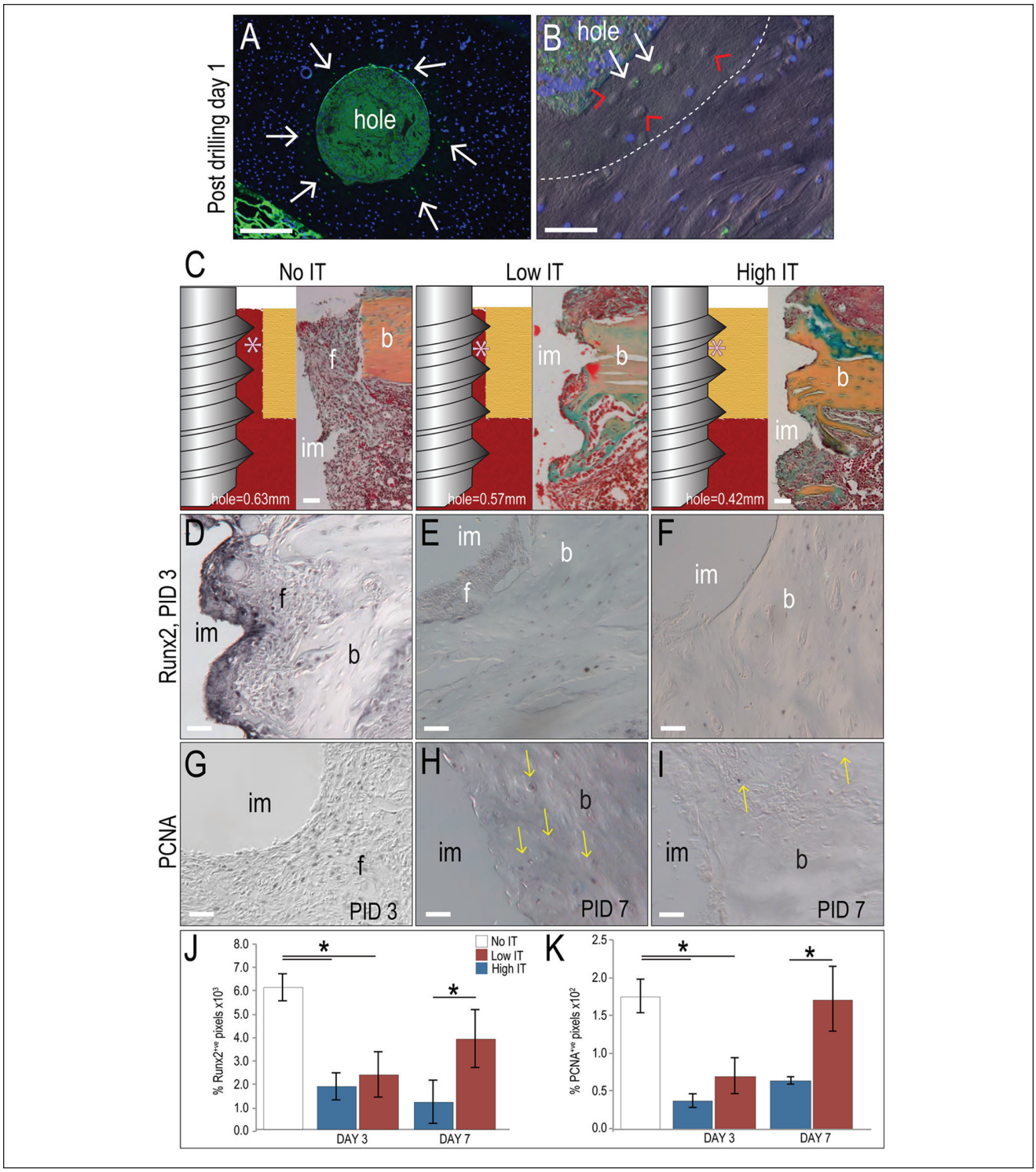

Figure 1. Characterization of peri-implant responses to low and high insertional torque (IT). (**A**) DAPI/TUNEL staining of the osteotomy site before implant insertion, in which osteocyte nuclei stain blue and cells undergoing programmed cell death stain green for TUNEL (arrows). (**B**) Dead osteocytes are indicated with red arrowheads. A dotted white line demarcates the zone of cell death. (**C**) Schematic of the osteotomy relative to the implant's external diameter. Asterisks mark gap between the peri-implant bone and implant. Runx2 immunostaining on representative tissue sections on PID3 in (**D**) no IT, (**E**) low IT, and (**F**) high IT cases. PCNA immunostaining on representative tissue sections on PID3 in (**G**) no IT, (**H**) low IT, and (**I**) high IT cases. Quantification on PID3 and PID7 in different IT environments of (**J**) Runx2 expression and (**K**) PCNA expression. im, implant; b, bone; f, fibrous tissue; IT, insertional torque; PID, postimplant day. Scale bar, 50 µm; $^{*}P < 0.05$. Quantification of Runx2 and PCNA expression are represented as mean ± SEM ($n = 4$). Differences were analyzed by Wilcoxon test.

Creating a Biological Model of Implant Misfit

We then evaluated how IT affected this zone of cell death. We created a situation of no IT, where the osteotomy was larger than the external diameter (ED) of the implant. By PID3, this gap was filled with fibrous tissue (Fig. 1C). Next we created a situation of low IT where the osteotomy was slightly smaller than the ED of the implant (Fig. 1C, low IT; see Appendix Table 1 for measurements and diameters). Then we created a situation of high IT where the osteotomy was significantly smaller than the ED of the implant, which resulted in the implant being fully engaged in the bone (asterisk, Fig. 1C; high IT). The mean IT values were 0 for the no-IT group, 0.05 ± 0.03 N-cm for the low-IT group, and 0.18 ± 0.02 N-cm for the high-IT group (Appendix Table 1).

We evaluated the molecular responses in different IT conditions. In no-IT cases, the osteogenic protein Runx2 was strongly expressed in peri-implant fibroblasts (Fig. 1D). In low-IT cases, weak Runx2 was detectable (Fig. 1E). In high-IT cases, Runx2 was found only in osteocytes (Fig. 1F). We quantified expression levels of Runx2 in the different IT environments and found that Runx2 was at its peak in the no-IT cases (Fig. 1J).

We evaluated mitotic activity in the peri-implant environment. Cell proliferation, as detected by immunostaining for proliferating cell nuclear antigen (PCNA; Waseem and Lane 1990), was highest in peri-implant tissues around implants placed with no IT (Fig. 1G). In low-IT cases, PCNA expression levels rose significantly between PID3 and PID7 (Fig. 1H), nearly reaching the same level of expression as was observed in the no-IT cases (Fig. 1K). In high-IT cases, PCNA expression was significantly lower and remained repressed relative to controls (Fig. 1I). Together, these data demonstrate that the lower the IT, the more the peri-implant environment favored cell proliferation and osteogenic differentiation.

FE Modeling of Interfacial Strain Created by Bone-implant Misfit

To provide quantitative information on the level of strain and stress created in low- and high-IT environments, we employed FE analyses. Bone was modeled as a disk of linearly elastic isotropic material ($E = 5$ GPa, $\nu = 0.33$) with $r = 2$ mm and thickness = 0.25 mm, and the outer periphery of the bone disk was fixed (Fig. 2A). These FE models were based on histology of the bone-implant interface (Fig. 2B).

Two FE models were used to simulate misfit between the internal diameter (ID) of the implant and the diameter of the osteotomy. In the low-IT model, the tips of the threads were initially engaged in bone to a depth of 15 μm, and then displaced an additional 5 μm to reach a total of 20 μm of misfit (Fig. 2C). This degree of misfit created a relatively small region of moderate strain (Fig. 2C). A similar pattern and magnitude of moderate strain could also be visualized via photoelasticity (Fig. 2D).

In the high-IT model, both the crest of the threads and the ID of the implant protruded into the bone (Fig. 2E). This degree of misfit created a large region of high strain at the thread crests and at the ID of the implant. The high strain state associated with high IT could also be qualitatively assessed via photoelastcicity using a stress Opticon (Fig. 2F).

Strain variations predicted by the FE models were plotted as a function of radial distance from the implant. In low-IT cases, the strains along the ID line were virtually zero (solid red line, Fig. 2G), and the strains along the OD line were initially high (~14%) but rapidly decreased as a function of distance (Fig. 2G). Approximately 100 μm from the thread crests, strains were <1% (red dotted line, Fig. 2G). In high-IT cases, the strains along the OD and ID lines were large (e.g., 15% to 20%) and were only minimally reduced as a function of distance. Even 200 μm into the bone, the strains remained as large as 5% (blue solid and dotted lines, Fig. 2G). Thus, the higher the IT, the greater the strain—in terms of its absolute magnitude and its distribution within the peri-implant bone.

The misfits in low and high IT cases corresponded to the degree of misfit described in clinical situations (see Appendix for references and details). Two distinct analytical models verified that the IT used in the mouse model was scaled appropriately to the recommended IT used to place dental implants in humans (Appendix Table 2). These analyses demonstrated that the interfacial pressures and strains for the mouse model correlated well with the IT used in clinical cases, thus validating the use of this mouse model for testing IT.

High IT and Its Associated High Strains Impedes Blood Flow and Causes Microfractures in the Cortical Bone

We evaluated cortical bone responses to low and high IT. In low-IT cases, there was uniform coloration of the bone (Fig. 3A); in high-IT cases, obvious blanching around the implant was noted (dotted line, Fig. 3B). On PID3, cortical bone around low-IT implants showed minimal evidence of disruption, except on the cut edge of the bone in contact with the implant (Fig. 3C). In contrast, small microfractures were evident in the bone adjacent to high-IT implants (arrows, Fig. 3D). Using Fuchsin staining (Burr and Hooser 1995), we found a significantly greater amount of microdamage in high-IT cases (Fig. 3E, F), which corresponded to sites of microcracks in the bone (arrows, Fig. 3F).

Microdamage can cause changes in cells connected via the haversian system (Burr et al. 1985); in keeping with

this, we observed significantly more dead and dying osteocytes around high-IT implants. Using DAPI to identify viable osteocyte nuclei and TUNEL to identify dying osteocytes, we found only a narrow zone (~60 µm) of damaged and dead osteocytes around low-IT implants (Fig. 3G, I). Around high-IT implants, the zone of TUNEL staining was twice as broad (Fig. 3H, J; quantified in Fig. 3K). Thus, placement of implants with high IT causes an immediate constriction in blood flow, creates microfractures in peri-implant bone, and causes extensive osteocyte death.

Active Bone Remodeling Occurs at the Bone-implant Interface

Microdamage acts as a stimulus for bone remodeling (Burr et al. 1985); consequently, we evaluated osteoclast and osteoblast activity in response to different strain profiles. In low-IT cases, there was no evidence of TRAP (osteoclast) activity; instead, the gap between the implant and bone on PID7 was filled with fibrous tissue (asterisk, Fig. 4A). In high-IT cases, there was abundant TRAP activity, especially near sites where the thread of the implant had cut into the cortical bone (dotted line, Fig. 4B). Around low-IT implants, ALP activity was high (Fig. 4C), indicating new matrix mineralization. In high-IT cases, ALP activity was restricted to osteocyte lacunae at some distance from the bone-implant interface (Fig. 4D).

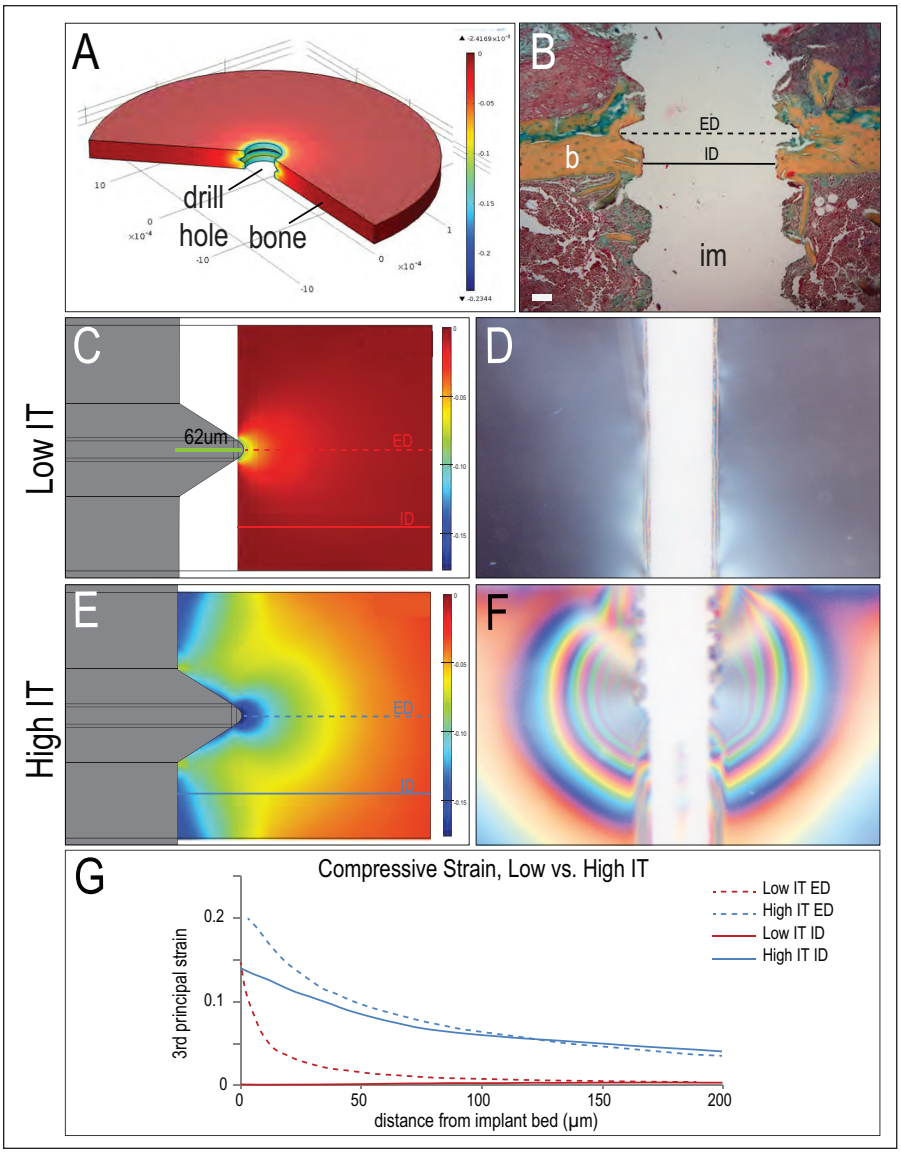

Figure 2. Relationships among IT, strain, and ostecyte death. (**A**) Three-dimensional finite element analyses showing the implant engaged in the bone disc and the resulting principal compressive strains. (**B**) Representative sagittal section stained with Pentachrome showing orientation of the implant in bone. (**C**) In low IT cases, contour plots of principal compressive strain fields and (**D**) Stress-Opticon (photoelastic) stresses. (**E**) In high IT cases, contour plots of principal compressive strain fields and (**F**) Stress-Opticon (photoelastic) stresses. (**G**) Dotted lines represent strain magnitudes measured from the implant crest radially outward into the cortical bone; solid lines represent the strain magnitudes measured from either the edge of the implant hole (C) or the bone-implant interface (E) outward into the cortical bone; compressive strain magnitudes are shown as positive values. Abbreviations as in Figure 1. Scale bar, 50 µm.

Bone Formation is More Pronounced around Implants Placed with Low IT

We observed new peri-implant bone in low-IT cases (Fig. 4E), which was absent in high-IT cases (Fig. 4F). Ten days later, when visualized under polarized light, Picrosirius red staining confirmed that, around low-IT implants, the peri-implant space was occupied by linearly arranged, yellow-orange collagen fibers (arrow, Fig. 4G). Around high-IT implants, the collagen fiber network was less organized (Fig. 4H). TRAP staining at this later time point revealed that a broad zone of newly formed bone around low-IT

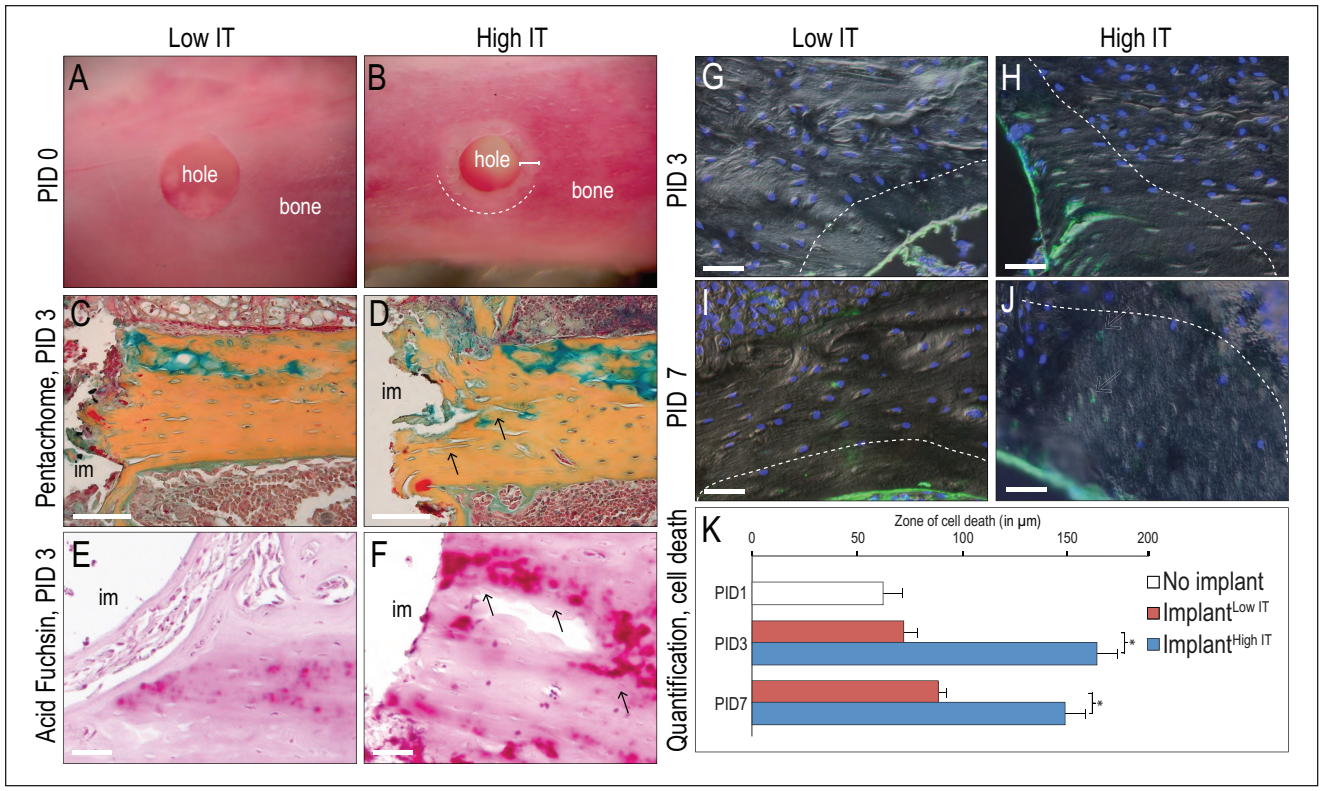

Figure 3. High IT causes microfracturing and increased osteocyte cell death. Peri-implant bone, imaged after removal of an implant placed with (**A**) low IT or (**B**) high IT. White bar, 140 µm. Representative Pentachrome-stained sections on PID3, where the implant was placed with (**C**) low IT or (**D**) high IT. Arrows indicate microcracks. Representative Fuchsin-strained sections on PID3, where the implant was placed with (**E**) low IT or (**F**) high IT. $DAPI^{+ve}$ nuclei and $TUNEL^{+ve}$ osteocytes on PID3, around implants placed with (**G**) low IT or (**H**) high IT. Co-stained images are superimposed on differential interference contrast images. DAPI and TUNEL staining on PID7, where the implant was placed with (**I**) low IT or (**J**) high IT. (**K**) Quantification of the zone of $TUNEL^{+ve}$ and $DAPI^{+ve}$ cells on PID1 in cases where an osteotomy was prepared (white bar), in low IT cases (red bars), and in high IT cases (blue bars). Histograms are represented as mean ± SEM ($n = 4$). Differences between high and low IT groups were analyzed by Wilcoxon test. Abbreviations as in Figure 1. Scale bar, 50 µm; $^{*}P < 0.05$.

implants was being actively remodeled to create a more lamellar structure (Fig. 4I). In contrast, the necrotic bone around high-IT implants was being resorbed (Fig. 4J).

High IT Adversely Affects Implant Osseointegration

We tested whether these cellular changes affected implant stability (Fig. 4K, L), using load and displacement plots (e.g., Fig. 4M). Peak-to-peak heights were measured and then divided to estimate a slope of the load-deflection plot; the slope was then multiplied to arrive at the value of EI as a measure of interfacial stiffness. A change in the deflection of the implant therefore indicated a change in the stiffness of the peri-implant material.

On PID1, low-IT implants showed the lowest stiffness, and high-IT implants exhibited greater stiffness (Fig. 4N). The stability testing was also performed on PID7; here, high-IT implants showed no improvement in stiffness, while low-IT implants showed a significant increase in interfacial stiffness (Fig. 4N).

Discussion

When placing an implant, clinicians typically use high IT to ensure that the maximum surface area of the implant is in contact with bone (Grandi et al. 2013). This high IT results in an implant with primary stability, which is considered a prerequisite for osseointegration (Moy et al. 2005). In clinical practice, the survival rate of these implants is good, which attests to the fact that bone has an enormous regenerative potential. There is an important caveat, however: in cases where the bone quality is suboptimal or the bone formation rate is slowed by a patient's systemic or metabolic disease or in cases of immediate and early loading, maximum peri-implant cell vitality is required to ensure osseointegration and implant stability.

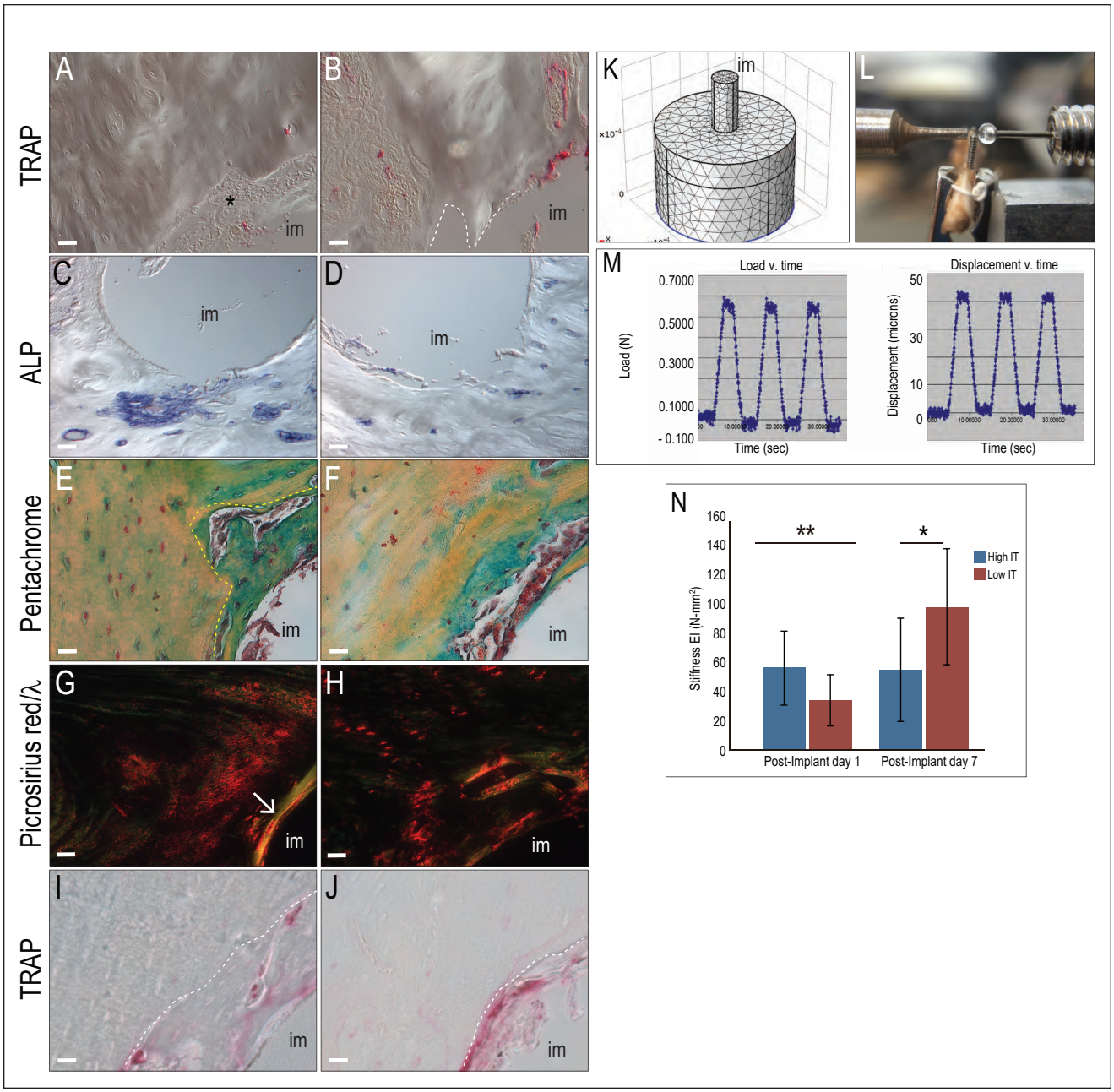

Figure 4. Insertional torque affects peri-implant bone remodeling and implant stability. (**A**) Representative tartrate-resistant acid phosphatase (TRAP)–strained tissue sections on PID7, where the implant was placed with low IT; the gap between the implant and the bone is filled with fibrous tissue (asterisk). (**B**) Representative TRAP-strained sections on PID7, where the implant was placed with high IT; dotted line identifies the bone cut by the implant thread. Representative ALP–strained sections on PID7, where the implant was placed with (**C**) low IT or (**D**) high IT. (**E**) Representative Pentachrome-strained sections on PID7, where the implant was placed with low IT; new bone formation is indicated with a dotted yellow line. Pentachrome stain distinguishes native mature (yellow-orange) bone from newer (blue-green) bone. (**F**) Equivalent section from a case where the implant was placed with high IT. (**G**) Representative tissue sections from PID17, stained with Picrosirius red and visualized under polarized light from a case where the implant was placed with low IT; the arrow indicates mature, linearly arranged, yellow-orange collagen fibers. (**H**) Representative tissue sections from PID17, from a case where the implant was placed with high IT. Peri-implant TRAP activity on representative tissue sections from (**I**) low and (**J**) high IT groups on PID17. (**K**) Design of implant-bone model for measuring stiffness. (**L**) The bone-implant stiffness test procedure where the mouse femur is clamped to a solid support. The load is applied perpendicular to the long axis of the implant. (**M**) Representative load and displacement plots as a function of time (s). (**N**) Bone-implant stiffness following placement of implants with low and high IT, measured on PID1 and PID7 (n = 5 for each condition; $^{*}P < 0.05$, $^{**}P < 0.01$). Abbreviations as in Fig. 1. Scale bars, 50 μm.

High IT and Its Relationship with Interfacial Strain and Primary Stability

Our data provide in vivo molecular, cellular, and histologic evidence linking high IT with the biological processes that predate implant failure. We identified spatial domains of strain created by high IT, which provided us with a map of peri-implant bone regions at risk for osteocyte apoptosis. In high-IT cases, strain at the bone-implant interface was >10% (Fig. 2), which is predicted to cause significant damage (Martin et al. 1998). Our molecular and cellular analyses (Figs. 3, 4), as well as the bone microdamage caused by high IT (Fig. 3), provide strong support for this conclusion.

Data in large animals (Nevins et al. 2012) and the clinical literature support these conclusions. In humans, implants placed with high IT are more likely to show signs of early loosening (Sennerby and Gottlow 2008) and radiographic bone loss at the implant-bone interface (Calandriello et al. 2003).

IT and the Timing of Implant Loading

Given these data, one might legitimately wonder why an implant placed with high IT actually succeeds. The answer lies in when implant stability is assessed. In cases of delayed loading, interfacial bone resorption likely occurs when the high-IT implants are submerged. In these cases, bone resorption acts as a stimulus for bone formation (Martin and Leibovich 2005), and implant loosening associated with the bone resorption is not manifested in a clinically observable manner.

The interplay of implant stability and IT comes into play more obviously in immediately loaded implants. In these cases, implants installed with high IT initially show primary stability because the maximal surface area of the implant is compressed into contact with bone. However, as the bone starts to resorb, the implant loses some stability (Fig. 4). If this implant has been subjected to immediate loading there is a high likelihood of implant micromotion, which can lead to further resorption and loosening. A key point is that the threshold between "high" torque and "dangerously high" torque depends on the actual strain magnitudes in bone—and their spatial extent—when a given level of IT is used.

Conclusions

Whether they are used as anchors for moving teeth or as a replacement for missing dentition, implants must be osseointegrated to be functional. Data presented here demonstrate how high IT generates strain in the peri-implant bone that is detrimental to osteocyte survival. High strains constrict blood flow and cause microdamage to the bone, both of which contribute to osteocyte necrosis, extensive bone remodeling, and minimal new bone formation. Although implants placed with high IT may exhibit primary stability, their ability to achieve secondary stability is uncertain.

Author Contributions

J.Y. Cha, A.A. Smith, J.B. Brunski, contributed to conception, design, data acquisition, analysis, and interpretation, drafted and critically revised the manuscript; M.D. Pereira, contributed to conception, design, data acquisition, analysis, and interpretation, drafted the manuscript; K.S. Houschyar, contributed to data acquisition, critically revised the manuscript; X. Yin, contributed to data acquisition and analysis, critically revised the manuscript; S. Mouraret, contributed to conception and design, drafted and critically revised the manuscript; J.A. Helms, contributed to conception, design, data analysis, and interpretation, drafted and critically revised the manuscript. All authors gave final approval and agree to be accountable for all aspects of the work.

Acknowledgments

This work is supported by grants from Yonsei University (6-2014-0090) to J-Y.C. and the California Institute for Regenerative Medicine (TR1-01249) to J.A.H. The authors declare no potential conflicts of interest with respect to the authorship and/or publication of this article.

References

Burr DB, Hooser M. 1995. Alterations to the en bloc basic fuchsin staining protocol for the demonstration of microdamage produced in vivo. Bone. 17:431–433.

Burr DB, Martin RB, Schaffler MB, Radin EL. 1985. Bone remodeling in response to in vivo fatigue microdamage. J Biomech. 18:189–200.

Calandriello R, Tomatis M, Rangert B. 2003. Immediate functional loading of Branemark System implants with enhanced initial stability: a prospective 1- to 2-year clinical and radiographic study. Clin Implant Dent Relat Res. 5 Suppl 1:10–20.

Cha JY, Kil JK, Yoon TM, Hwang CJ. 2010. Miniscrew stability evaluated with computerized tomography scanning. Am J Orthod Dentofacial Orthop. 137:73–79.

Deguchi T, Takano-Yamamoto T, Kanomi R, Hartsfield JK Jr, Roberts WE, Garetto LP. 2003. The use of small titanium screws for orthodontic anchorage. J Dent Res. 82:377–381.

Duyck J, Corpas L, Vermeiren S, Ogawa T, Quirynen M, Vandamme K, Jacobs R, Naert I. 2010. Histological, histomorphometrical, and radiological evaluation of an experimental implant design with a high insertion torque. Clin Oral Implants Res. 21:877–884.

Esposito M, Grusovin MG, Maghaireh H, Worthington HV. 2013. Interventions for replacing missing teeth: different times for loading dental implants. Cochrane Database Syst Rev. 3:CD003878.

Grandi T, Guazzi P, Samarani R, Grandi G. 2013. Clinical outcome and bone healing of implants placed with high insertion torque: 12–month results from a multicenter controlled cohort study. Int J Oral Maxillofac Surg. 42:516–520.

Higuchi K, Block MS. 2000. Orthodontic applications of osseointegrated implants. Chicago (IL): Quintessence.

Leucht P, Kim JB, Wazen R, Currey JA, Nanci A, Brunski JB, Helms JA. 2007. Effect of mechanical stimuli on skeletal regeneration around implants. Bone. 40:919–930.

Martin P, Leibovich SJ. 2005. Inflammatory cells during wound repair: the good, the bad and the ugly. Trends Cell Biol. 15:599–607.

Martin RB, Burr DB, Sharkey NA. 1998. Skeletal tissue mechanics. New York (NY): Springer.

Minear S, Leucht P, Jiang J, Liu B, Zeng A, Fuerer C, Nusse R, Helms JA. 2010. Wnt proteins promote bone regeneration. Sci Transl Med. 2(29):29ra30.

Moy PK, Medina D, Shetty V, Aghaloo TL. 2005. Dental implant failure rates and associated risk factors. Int J Oral Maxillofac Implants. 20:569–577.

Nevins M, Nevins ML, Schupbach P, Fiorellini J, Lin Z, Kim DM. 2012. The impact of bone compression on bone-to-implant contact of an osseointegrated implant: a canine study. Int J Periodontics Restorative Dent. 32:637–645.

Sennerby L, Gottlow J. 2008. Clinical outcomes of immediate/early loading of dental implants. A literature review of recent controlled prospective clinical studies. Aust Dent J. 53 Suppl 1:S82–S88.

Trisi P, Todisco M, Consolo U, Travaglini D. 2011. High versus low implant insertion torque: a histologic, histomorphometric, and biomechanical study in the sheep mandible. Int J Oral Maxillofac Implants. 26:837–849.

Waseem NH, Lane DP. 1990. Monoclonal antibody analysis of the proliferating cell nuclear antigen (PCNA). Structural conservation and the detection of a nucleolar form. J Cell Sci. 96(Pt 1):121–129.